HEAT-INDUCED LASER DRIFT: INVESTIGATING THE INFLUENCE OF HEAT SOURCES ON THE LLE TRANSPORT MIRROR STRUCTURE

Linh Vu **Owen Wacha** **Gyeongjae Yoo** **Makarii Yurkiv**

ABSTRACT

Micrometer-scale laser drift in the Omega-60 laser system at the Laboratory for Laser Energetics (LLE) may be hindering their fusion technology research. The prevailing drift hypothesis is that stray thermal sources intermittently heating the steel beams of the transport mirror support structure cause the mirrors to tilt. Two controlled heating experiments were conducted to test the hypothesis, one on a freely damped table and one involving a large steel beam. Experiments and associated finite element analysis (FEA) simulations yielded micrometer-scale drifts when subjected to thermal conditions like those seen at LLE. The experimental drift value was computed to be **6.018 mm** while the FEA model displayed **2.002 mm** of drift.

Simulation of the transport mirror structure inspired by thermal data shows interesting drift results as well. Analysis of drift data collected by LLE inspired other potential drift sources to be investigated in the future. The thermal structural analysis of the transport mirror structure at LLE demonstrated drifts due to rotations of the mirrors. The drift value computed from the thermal FEA was **16.917µm** with **0.98%** error compared to the drift value of mirror 30 from the ultraviolet laser stability test results, 17.092µm. However, the drift values of all the other mirrors had over 33% error compared to the LLE's stability data. This indicates that there are more sources of heat that was not captured or there are other possible sources that can affect the drifting behavior of the laser, which will be discussed later in the document.

PROBLEM DEFINITION

The Laboratory for Laser Energetics (LLE) is developing nuclear fusion technology and exploring the fundamental science of fusion using Omega-60 Laser System, that focuses up to 40,000 J of energy using a laser on a sample in about one nanosecond [1]. The laser system control requires high-precision optical measurements and stability monitoring as it needs to hit a target smaller than one millimeter in diameter [1]. According to the ultraviolet targeting stability test report by J. Kwiatkowski at LLE (2020), the lasers in the Omega-60 are experiencing drift, which seems to be the effects of the environment surrounding the laser system. The sources of these drifting behaviors must be identified to find a method to minimize the drift or to remove these behaviors.

REQUIREMENTS, SPECIFICATIONS, DELIVERABLES

Table 1: Project deliverables, requirements, and specifications

Deliverables	1	Technical Report with simulations and test data			
	2	Appropriate experimental set-up to measure drifts			
Requirements	1	Improve LLE's understanding of drift sources			
	2	Model thermal effects on transport mirrors			
	3	Test hypothesis of stray heat sources in the chamber affecting the transport mirrors			
Specifications		Value	Unit	Description	Method of evaluation
	1	1	μm	The magnitude of drift caused by a thermal source	Simulations and Experiments
	2	0.1	°C	Maximum increase in ambient temperature due to measurement apparatus	Thermal camera

CONCEPTS

One of the two key deliverables for the project is an appropriate experimental setup (Table 1). The goal of the setup is to demonstrate that the transport mirror structure subjected to heat would deform and displace mirrors enough for the laser drifts like those that have been observed at LLE. To achieve a similar temperature profile as seen in thermal images from the OMEGA-60 target chamber room, a thermal load will be applied to the steel beam using a Kapton heater. The setup would also involve a mirror attached to a steel beam and a device that allows for the calculation of the change in the mirror's orientation. As the steel beam is heated and deformed, the mirror is expected to move. Discussed below are the four ways to measure the change in orientation of the mirror.

1. Autocollimator

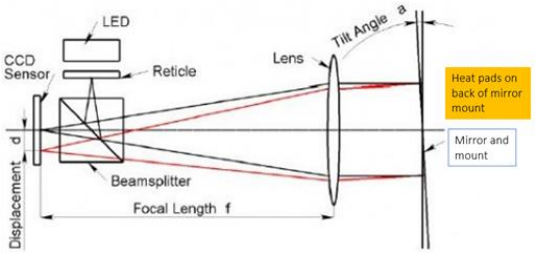

Figure 1: Working mechanism of an autocollimator

An Autocollimator is an instrument that measures angular reflections with high precision [2]. The device projects a reticle

pattern as a collimated beam to a mirror in front of it. The collimated beam is then reflected to the autocollimator's charged-coupled device (CCD) sensor, generating the collimated image. The x and y displacements of the autocollimation image are measured, which are proportional to the mirror's tilt angle. An advantage of an autocollimator is that it is easy to use and to implement. However, it needs to be placed approximately 2.5 cm (about 1 in) away from the mirror surface to achieve a high-resolution image with extremely small displacements, which is currently not possible in the actual OMEGA-60 Laser target chamber where the mirrors are located [2].

2. Pointing Laser and Quad Cell

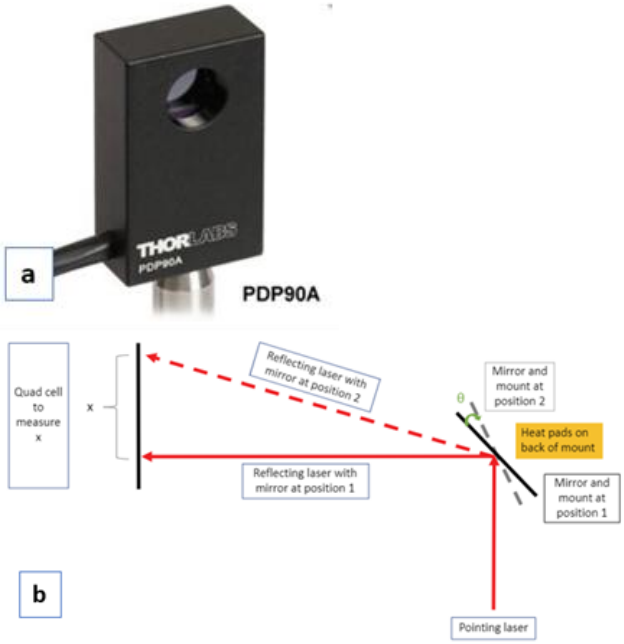

Figure 2: (a) PDP90A Lateral Effect Position Sensor [3], (b) Laser and quad cell set-up diagram

Another concept for the experimental setup is to use a pointing laser and a quad cell (LQC). This setup consists of a pointing laser aimed at the mirror which reflects the laser back to a quad cell located at a certain initial point (Figure 2b). As the mirror mount gets heated up by the Kapton heaters, it will deform and move at an angle of θ, changing the reflection angle of the laser, as well as the point where the laser hits the quad cell. The displacement between the two points where the laser hits the quad cell, before and after the mirror tilted θ degrees, is measured by the quad cell. Using this distance, the angle of deformation, θ, can be calculated.

The advantage of this setup is that the laser can be positioned far away from the mirror to get more accurate measurements and will not interfere with LLE's experiments. Additionally, quad cells with high resolutions of under 1 µm (specified in Table 1) are relatively inexpensive. One such quad cell is the PDP90A Lateral Effect Position Sensor produced by THORLABS (Figure 2a), with the cost of $451.88. This quad cell can measure changes in laser position as small as 0.75 µm, which satisfies our specification of measuring at least 1 µm of drift and identifying the associated sources.

3. Interferometer

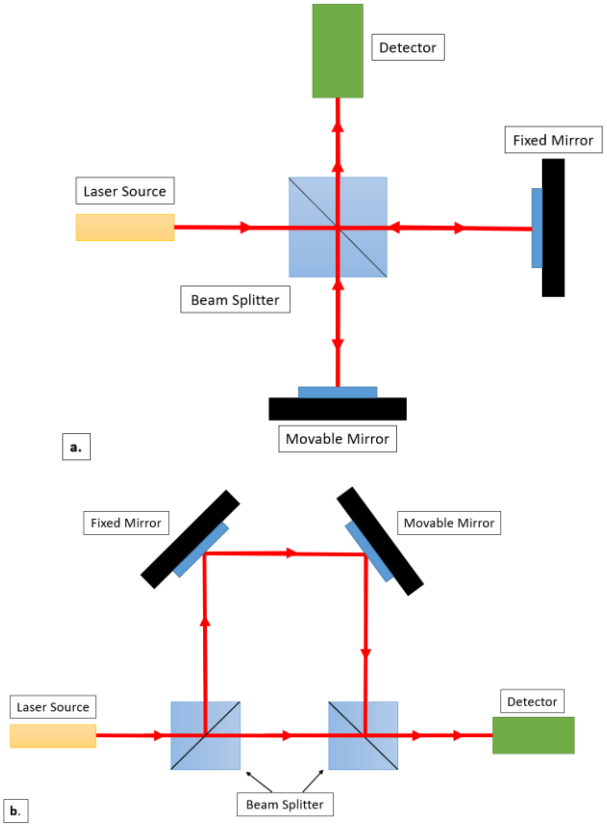

Figure 3: (a) Michelson Interferometer, (b) Modified Mach-Zehnder Interferometer

An interferometer measures small distances, changes, or other properties of an object by studying the way light waves combine or "interfere" with each other [4]. It works by splitting a beam of light into two separate beams, directing them along different paths, and then recombining them [4]. When the light beams meet again, they create a pattern that depends on the difference in their paths called fringes [4]. By analyzing these fringes, accurate information about the object can be gathered. Interferometers are incredibly precise instruments, capable of measuring extremely slight changes or distances [4]. The level of precision depends on the specific type of interferometer and its application, but in general, they can detect variations down to the level of a fraction of the wavelength of light used, which can be as small as a few nanometers [4]. This makes them valuable for this specific experiment as they can measure the tip/tilt of a mirror down to the precision of at least a micron, which meets our specifications [4].

4. MEMS Inclinometers

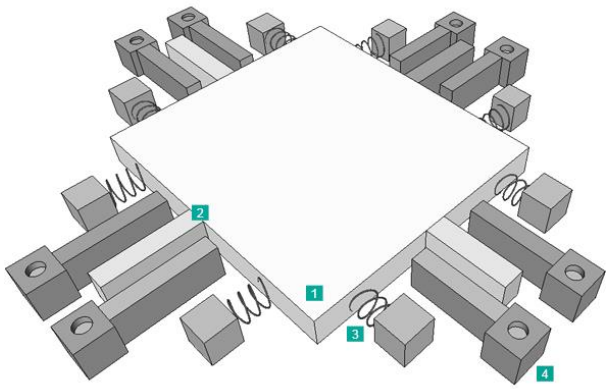

Figure 4: Mechanism of the MEMS inclinometer composed of mass (1), electrodes on the mass (2), springs (3), and fixed electrodes (4)

The MEMS inclinometers are directly attached to the object of interest. They compute the orientation angle of an object by using an elastic support structure system with a tiny mass suspended within it, which is moved due to gravity as the object tilts [5]. The moved mass causes a capacitance used to calculate the tilt angle between the electrodes attached to the mass (2) and the fixed electrodes (4) on the supporting structure [5]. The advantage of using this device is that the tilt of the mirror can be measured with extremely high precision [5]. Also, no additional set up is required as the inclinometer can be attached right onto the mirror to measure the displacement [5]. However, a high-resolution inclinometer needed to measure small displacements down to microns can cost over $1000, exceeding the given budget of this project [5].

Decision matrix and discussion

Table 2: Pugh decision matrix of the four experimental setups

	Inclinometer	LQC	Autocollimator	Interferometer
Ease of implementation	0	-1	-1	-1
Applicability to OMEGA-60	0	+1	-1	+1
Resolution	0	+1	+1	+1
Ease of Access	0	0	+1	+1
Cost	0	+1	+1	+1
Total	0	+2	+1	**+3**

All the equipment had the capability to measure in high resolution, but the interferometer setup was selected as the setup to be used for the experiment because it excelled in most of the categories that were considered with the highest precision out of all the equipment discussed previously according to Edward Herger, senior lab engineer in the Institute of Optics at the University of Rochester.

TEST PLAN

Rettner Hall, at the University of Rochester, was selected as the most optimal location to hold the experiment. The structural support beams of Rettner Hall are exposed large steel I-beams, with the whole structure of connected beams vaguely resembling the north/south end mirror structures at LLE. Additionally, Rettner has a large open atrium with long distances, which can allow for more detailed drift measurements and for data collection without interruption.

However, due to the electrical and HVAC systems, Rettner Hall was expected to experience large vibrations, which could add error to the measurements. Additionally, the size of the atrium had the potential for larger temperature fluctuations due to uneven temperature control. Moreover, the team was initially unfamiliar with how to set up and operate an interferometer. Therefore, it was decided to have a separate experimental setup with the interferometer in an optics laboratory. This setup would allow for vibration isolation of the interferometer as it would be placed on a passively damped optical table. The temperature fluctuations would be reduced, as the lab is temperature controlled and smaller in size. And it would also allow the team to become familiar with operating an interferometer and taking fringe measurements before executing the large experiment in Rettner. The optical bench setup would serve as the ideal version of the heating experiment and as a proof of concept, as it would show whether displacement due to heating can have a significant effect on mirror drift.

Optical Bench Setup

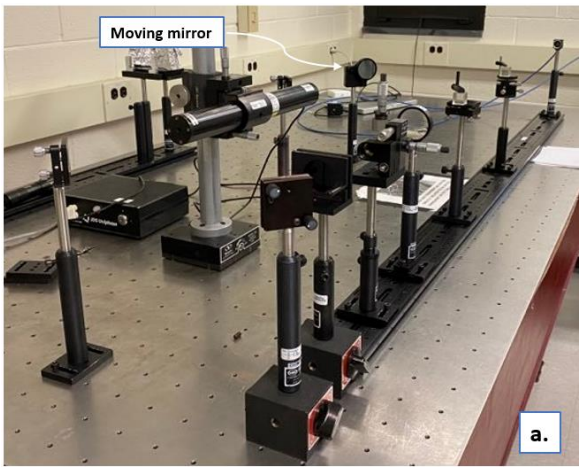

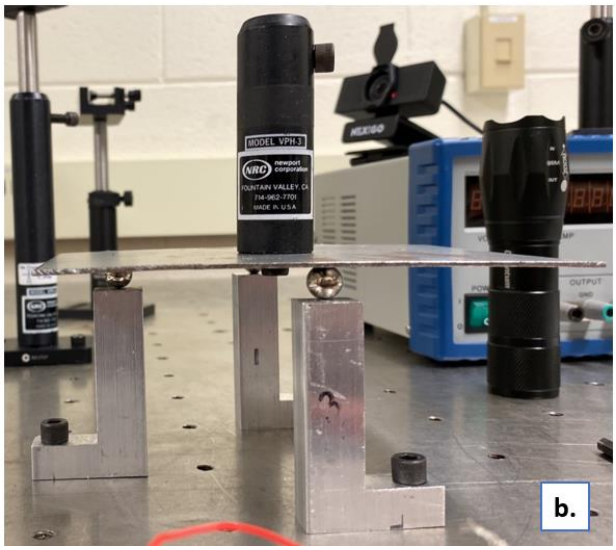

Figure 5: Optical Bench Setup (a) Mach-Zehnder Interferometer Setup in Optical Bench, (b) Kinematic 3-stage mount for the moving mirror

The optical bench setup utilized a modified version of the Mach-Zehnder Interferometer (Figure 5a) located on a vibration-isolated optical table. The components include a He-Ne laser source, a redirecting mirror, a spatial beam filter, a collimated lens, two beam splitters, a fixed mirror, a movable mirror, and a fringe detecting camera. After being fired, filtered, and collimated, the laser went through a two-beam splitter and two-mirror system before recombining and hitting a stationary camera. The interference of the reflected and transmitted beams created fringes, which were observed and recorded using the camera.

For the purposes of this experiment, the movable mirror mount was positioned on top of a steel plate kinematically supported by 3 aluminum L-blocks (Figure 5b). Kinematic support was used to make sure the steel plate always remained in the same position with each run of the experiment with high repeatability. One of the L-blocks was heated using a Kapton heater and then cooled from the free air convection of the room. As the block was heated, it was expanding, making the steel plate tilt. Therefore, the tilt of the moveable mirror can be approximated as the tilt of the steel plate. Any tip/tilt of the movable mirror is reflected in the fringe movement, hence the tilt resulting from heating the aluminum L-block can be calculated by using the change in fringe spacing. Using the distance of **0.381 m** between the moving mirror and the beam splitter together with the tilt angle of the mirror, drifts were calculated. A MATLAB code was written to process and analyze the fringe data recorded by the camera. The output of the code generated the fringe angle and the fringe spacing of each fringe image. The changes in these two parameters were then used to calculate the tilt angle of the movable mirror.

Rettner Setup

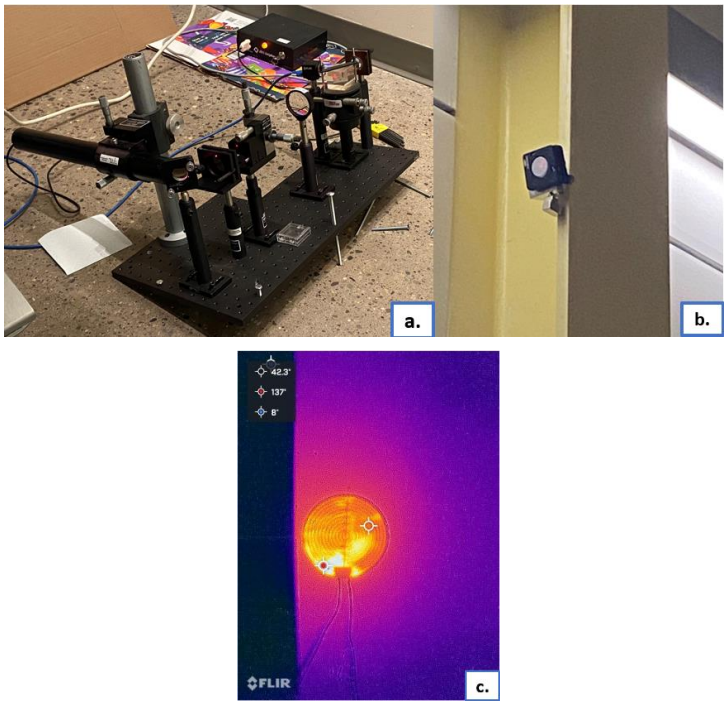

Figure 6: Rettner setup (a) Fixed components of the interferometer (b) Movable mirror (c) Kapton heater thermal image

On the Rettner setup, the movable mirror was attached to a steel beam. This induced spatial limitations for the camera and the mirror placements because the movable mirror location in the Mach-Zehnder Interferometer must be placed so that the laser reflects off the mirror at a 45° angle relative to the mirror surface. However, in a Michelson Interferometer (Figure 3a), the mirrors are oriented so that the laser reflects off the movable mirror perpendicular to the surface, which enables all the fixed components to be on one optical breadboard. The use of Michelson interferometer for the Rettner experiment allowed the adjustment of the movable mirror position without interrupting other components of the setup.

All fixed components were attached to an optical breadboard and placed on the floor in Rettner Hall. The fixed components include a He-Ne laser source, a redirecting mirror, a spatial beam filter, a collimated lens, a beam splitter, a fixed mirror, and a fringe detecting camera. After being fired and collimated, a one-inch diameter laser transmitted partially to the fixed mirror and reflected partially to the movable mirror through a beam splitter. The two partial laser paths reflected to the beam splitter and interfered. This interference produced fringes and was recorded by the camera.

To attach the movable mirror on a steel I-beam in Rettner without damaging the beam's structure, a kinematic magnetic adapter was designed and manufactured. Since the I-beam was directly subjected to a heat source and deformed, the movable mirror mounted on the beam should move with respect to the

beam's deformation with high repeatability. Therefore, the kinematic constraints were desirable. The mirror mount was screwed into the aluminum adapter, and the adapter was kinematically attached to the steel beam through six points of contact allowing zero degrees of freedom (Figure 6b).

Initially, the movable mirror was placed at the bottom of the I-beam and the interferometer was set up so that the laser was parallel to the ground. However, this was deemed to be limiting for achieving the desired results because the displacement near the fixed ends of a beam is much smaller than the middle of the beam. Therefore, the movable mirror was moved **2.895 m** upwards near the middle point of the beam and was angled down by manipulating the orientation of the mirror mount. The interferometer was tilted upwards using a bolt and moved to **11.815 m** away from the I-Beam so that the laser hits the mirror perpendicularly (Figure 6a). Then the Kapton heaters were attached to the bottom of the beam with 10V applied and the fringes were recorded from around 12:00 am to 8:30 am. The same process was performed with 20V. The recorded fringes data were then processed and analyzed using the same MATLAB code used in the optical bench experiment.

MECHANICAL ANALYSIS AND CALCULATION

LLE North-End Transport Mirror Structure FEA

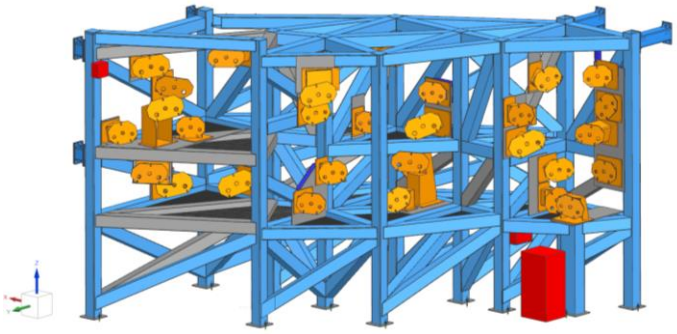

Figure 7: LLE's Transport Mirror Structure with Heat Sources (3 red blocks)

A thermal finite analysis was performed on the LLE's transport mirror structure. The thermal loads were placed on the structure after analyzing thermal images of various heat sources that were taken inside the target bay. The thermal images were taken using a FLIR thermal camera inside the LLE's target bay area. The major heat sources (Appendix III) were located on the bottom right corner of the structure and at the top left which can be seen in Figure 7. All the sources of heat were electronic devices that were located near the transport mirror structure.

Modeling heat transfer from the sources to the structure using radiation and convection was extremely complex to accurately model through FEA. Also, the structure was too complex and large to run simulations. To simplify the model, the transport mirror structure was idealized as a wire frame structure. In addition, thermal loads were applied directly to the part of the structure near the heat sources, and the power of the heat sources were adjusted so that the temperature change on the structure does not exceed +0.2˚C from the controlled temperature of the target bay, which is 20 ± 0.1˚C. The boundary conditions of the simulation can be found in Appendix II.

Below in Figure 8, is the temperature profile of the structure after being heated for 8 hours. The maximum temperature observed on the structure was 20.150 ˚C. The small heat source on the top left side of the structure on figure 7 did not seem to affect structure as much as the ones at the bottom right. Therefore, center points of the mirrors, that are located on the left side of lower level of the structure, were added in as a point to visualize and collect displacement and rotation data.

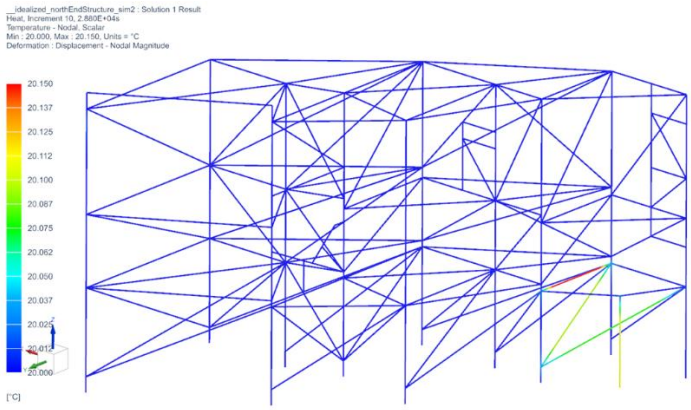

Figure 8: Temperature profile of the transport mirror structure with heat applied to the structure

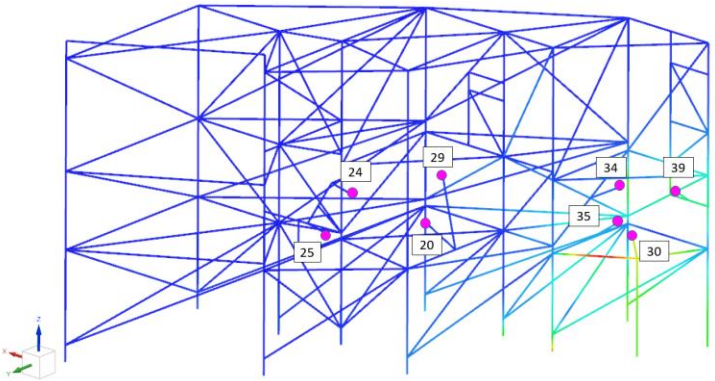

Figure 9: Magnitude of overall Rotation in the Transport Mirror Structure members due to Heat Sources with 8 magenta circles that represent the center point of the transport mirrors numbers corresponds to the mirror ID number.

Table 3: Transport Mirror Rotation from its original position [μdeg]

Mirror ID	$d\theta_x$	$d\theta_y$	$d\theta_z$
24	-0.2696	3.896	-2.007
25	-0.2604	3.613	-2.039

29	1.855	3.412	-10.34
20	1.855	3.412	-10.34
30	64.28	53.42	65.16
39	-65.03	-7.611	10.78
34	13.92	6.38	14.26
35	4.072	6.741	41.18

The analysis focused on the rotation of the mirror as the translation of the mirror does not change the angle of the reflected laser since it is designed to be as flat as possible. The displacement data can be found in Appendix II. The overall magnitude of the rotation can be seen in figure 9. Specific values of the rotations about each axis acquired from the thermal FEA can be found on table 3.

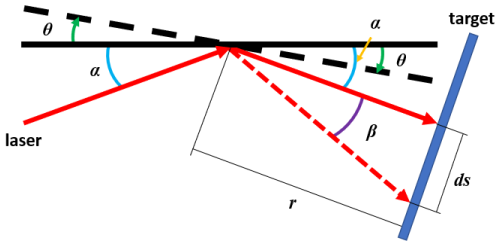

Figure 10: Diagram demonstrating relationship between drift of the laser to the tilt of the mirror

The angle between the original beam path and the new beam path, β, is computed as follows.

$$\beta = \alpha + \theta - (\alpha - \theta) = 2\theta \quad (1)$$

where α is the original incident and reflecting angle and θ is the mirror tilt angle. Drifting distance, ds, can be calculated by using the using the equation below,

$$ds = r \cdot tan(\beta) \quad (2)$$

along with mirror rotation values from table 3, the drift values are computed in Table 4.

Table 4: Laser Drift due to the Rotation of the Transport Mirror [μm]

Mirror ID	dx	dy	dz	Magnitude
24	-0.07248	1.04742	-0.53957	1.18045
25	-0.07564	1.04951	-0.59229	1.20747
29	0.39325	0.72333	-2.19205	2.34157
20	0.42943	0.78987	-2.39370	2.55697
30	10.26102	8.52744	10.40149	16.91735
39	-8.15518	-0.95447	1.35188	8.32139
34	1.90825	0.87462	1.95486	2.86843
35	0.60623	1.00359	6.13080	6.24191

Fatigue Analysis

Due to the nature of this project, fatigue analysis is not applicable.

Fastener Torque Calculation

To properly fasten the L-blocks to the optical table for the optical bench experiment, a fastener torque calculation was performed. The fastener used for this setup was a 1/4"-20 stainless steel cap screw. The fastener torque for a bolted connection can be described using the following equations.

$$T = KF_i d \quad (3)$$

where K is material dependent, F_i is the preload, d is the nominal diameter of the bolt. K for this fastener is around 0.2 (stainless steel into aluminum 6061) and the diameter is 0.25 in.

$$F_i = 0.9F_p \quad (4)$$

where F_p is the proof load. For a ¼ inch stainless steel socket head cap screw,

$$F_p = 0.4D \quad (5)$$

where D is the design load (here tensile load) of 3,420 lb_f. From this the proof load and preload become,

$$F_p = 0.4 \cdot 3420\,[lb_f] = 1368\,[lb_f]$$

$$F_i = 0.9 \cdot 1368\,[lb_f] = 1231.2\,[lb_f]$$

Therefore, the minimum fastener torque is computed as **61.65** $[\boldsymbol{lb_f \cdot in}]$ or **5.13** $[\boldsymbol{lb_f \cdot ft}]$**.**

L-block thermal expansion Analysis

The Kapton heater used in the optical bench experiment had a resistance of 99.5 Ω. The maximum voltage used in the experiment was 40 V. Assuming all power went towards producing heat, the rate of heat developed by the Kapton heater was:

$$\dot{Q} = \frac{V^2}{R} = \frac{(40V)^2}{99.5\Omega} = 16.08\,[W] \quad (6)$$

For each run of the experiment a steady-state temperature was reached. At steady state, the rate of heat transfer from conduction and convection was the same. So, the rate of heat transfer from the Kapton heater equaled the rate of heat transfer from convection, 16.08 W. The rate of heat transfer from convection equation is as follows:

$$\dot{Q} = hA_s(T_s - T_\infty) \quad (7)$$

where h is the heat transfer coefficient, A_s is the surface area of the block under convection, T_s is the surface temperature of the block, and T_∞ is the ambient temperature.

The heat transfer coefficient for free convection by air varies from $2.5\ \frac{W}{m^2 \cdot K}$ to $25\ \frac{W}{m^2 \cdot K}$ and the ambient temperature in the room was around $20\ °C$. The surface area of the block is

measured to be 0.005382 m^2. Therefore, the surface area temperature of the L-block was calculated using the equation below. To achieve a reasonable temperature of the L-block, the free air convection coefficient was chosen to be $25\ \frac{W}{m^2 \cdot K}$.

$$T_s = T_\infty + \frac{\dot{Q}}{hA_s} = 139.5°C \tag{8}$$

Assuming that the temperature of the L-block at steady-state is uniform throughout, the final temperature of the L-block was calculated to be $139.5°C$.

To find the change in height of the L-block the following equation was used:

$$\Delta H = H_0 \cdot CTE \cdot \Delta T \tag{9}$$

where H_0 is the initial height of the block, CTE is the coefficient of thermal expansion of the block, and ΔT is the change in temperature. The initial height of the block was 2.43 inches, the CTE of aluminum 6061 is about $23.4\ 10^{-6}/°C$, and the change in temperature was $139.5°C - 20°C = 119.5°C$. Using Equation (7), the change in height of the heated L-block, ΔH, is calculated to be **0.006796 in** or **172.62 μm.**

Using geometrical calculations, the distance from the L-block that is being heated to the axis of rotation of the steel plate was calculated to be 3.58 inches. This distance and the change in height form a right triangle from which the tilt of the steel plate can be calculated:

$$\theta = \tan^{-1}\left(\frac{0.006796\ in}{3.58\ in}\right) = 0.109° \tag{10}$$

The plate, and therefore the mirror was calculated to tilt **0.109°** from one of the L-blocks being heated by a Kapton heater. These theoretical results will be compared with the simulation and experimental results later.

Tolerance Analysis

For the manufacture of the Rettner setup's aluminum adapter, the holes needed to be drilled to press fit steel pins into. To find the appropriate drill size for the holes, a tolerance analysis was performed.

From the manufacturer, the diameter of the pins is $\frac{3}{16}\ [in] \pm 2.5\%$. A shaft-based press fit implies a **P7/h6** fit designation. Additionally, the following formulas apply,

$$D_{min} = D - \delta_f \tag{11}$$

$$D_{max} = D - \delta_f + \Delta D \tag{12}$$

where D, D_{min}, and D_{max} are the basic, minimum, and maximum sizes of the holes, ΔD is the tolerance grade for hole, and δ_f is the fundamental deviation.

Using Table, A-14 (Shigley's) and the **P**7 designation, δ_f was found to be 0.0005 inches. Using Table, A-13 (Shigley's) and the P**7** designation, ΔD was found to be 0.0005 inches. Using equations (9) and (10), the best size of the holes was calculated to be ranging from 0.1870 to 0.1875 in.

To drill a hole of the required diameter, a **size-13 drill (0.1850 in)** was chosen, as the standard drilled hole tolerance is +0.004/-0.001 in, and the calculated press fit hole falls best in that range.

Fringe-Related Drift Calculation

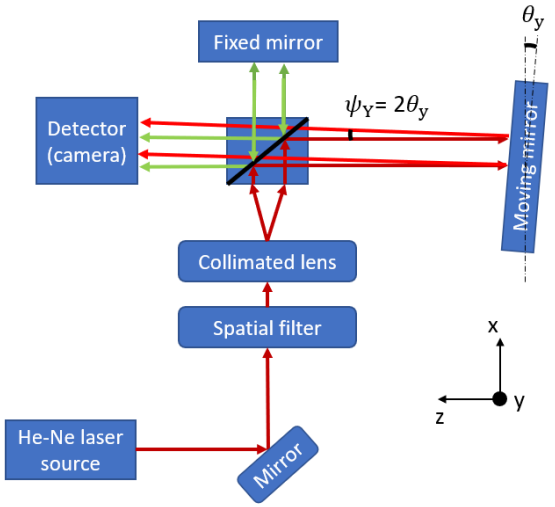

Figure 11: Rettner's Michelson Interferometer Setup

Figure 11 shows the diagram of the Michelson interferometer in Rettner setup as if the movable mirror is tilting at an angle of θ around the y axis. Let the baseline position be where the moving mirror is having $\theta_{x,y} = 0°$. The rotations around the x and y axes correspond to drifts in the y and x directions, respectively.

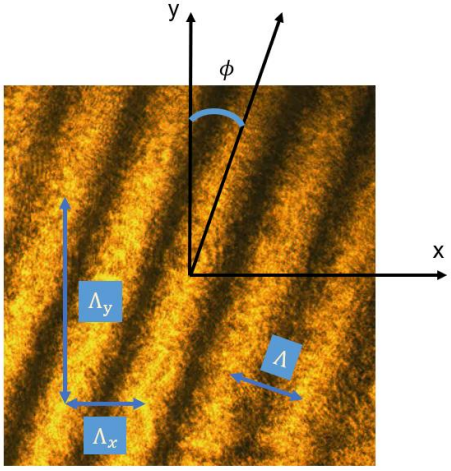

Figure 12: Fringe Diagram. This fringe image was collected from the initial levelled Rettner experiment with a 30V-1.26A or 37.8W heat source through a 24Ω Kapton heater

On a fringe image (Figure 12), there are four parameters under consideration including: Λ is the absolute fringe spacing measuring from the centroid of one fringe to the adjacent one in the direction perpendicular to the fringes' axis; Λ_x and Λ_y are distances between one fringe's centroid to another's in x and y directions respectively; and ϕ is the angle between the axis parallel to the fringes and the y axis. The relationship between these four parameters is described through the equations below.

$$\frac{1}{\Lambda^2} = \frac{1}{{\Lambda_x}^2} + \frac{1}{{\Lambda_y}^2} \tag{13}$$

$$\tan\phi = \frac{\Lambda_x}{\Lambda_y} \tag{14}$$

According to Equation (13) and (14), if the absolute fringe spacing, Λ, and the angle ϕ are given, then the fringe spacing in x and y directions can be calculated.

$$\Lambda_x = \Lambda \cdot \sqrt{(\tan\phi)^2 + 1} \tag{15}$$

$$\Lambda_y = \Lambda \cdot \sqrt{\frac{1}{(\tan\phi)^2} + 1} \tag{16}$$

Figure 11 indicates that a tilt movement of any angle θ around an axis of the moving mirror results in a change of 2θ around the same axis in the incoming laser beam of the detector. This resultant angle change is called ψ:

$$\psi_{x,y} = 2 \cdot \theta_{x,y} \tag{17}$$

To correlate the mirror movement to the fringe movement, a relationship between the fringes' spacing, Λ_x and Λ_y, and the tilt angle of mirror, θ_x and θ_y, is developed.

$$\theta_{x,y} = \frac{\lambda}{2\Lambda_{x,y}} \tag{18}$$

where λ is the wavelength of the laser source. The rotations around the x and y axes provide the drift amounts over a certain distance. With the distance of L between the moving mirror and the camera detector, the drifts in x, y, and in total, are calculated as follows.

$$d_{x,y} = L \cdot \tan(2 \cdot \theta_{y,x}) \tag{19}$$

$$d_{total} = \sqrt{{d_x}^2 + {d_y}^2} \tag{20}$$

Fringe Video Processing Code

Based on the previous calculation the key pieces of data to be extracted from fringe videos are the angle ϕ and the fringe spacing Λ. The fringe videos of the Rettner experiments were processed using MATLAB code based primarily on a 2-dimensional Fast Fourier Transform (FFT) analysis method. The FFT yields ϕ and the image is then rotated to get the fringes oriented vertically. Once vertical the fringe spacing is determined using the mean distance between fringe peaks. The FFT method yielded the most consistent results across several different approaches that were attempted including Hough transform, image thresholding, line detection, and a custom angle finder algorithm.

Optical Bench Setup FEA

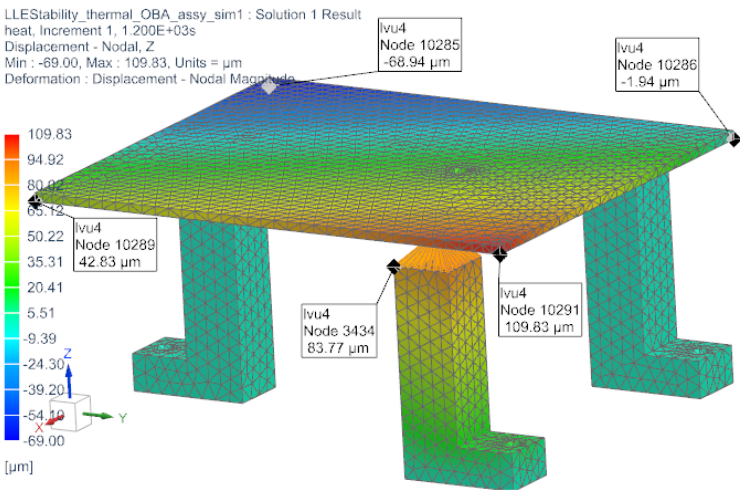

Figure 13: Displacement of the steel plate in Z-direction due to the heating in the front block. (Note: The displacement in X and Y can be found in Appendix IV)

The Optical bench setup was modeled using Siemens NX. A thermal FEA was performed on the setup to observe the impact Kapton heater heating has on an aluminum L-block which can be observed by the tilt of the mirror attached to the steel plate. Using the results from this FEA, a theoretical angle of tilt of the mirror was calculated. The thermal FEA assumed an applied thermal load of 16.08 W and convective cooling by air with a heat transfer coefficient of $25\ \frac{W}{m^2 \cdot K}$, like the applied parameters in the theoretical mechanical analysis on the L-block thermal experiment above. The L-block was heated for over 20 minutes in both the FEA simulation and experiment. The boundary conditions of the FEA model are demonstrated in Appendix IV.

According to the FEA calculations, the mirror tilted **0.0564°** with respect to the z-axis, and the heated L-block grew **83.77 μm** in the z-direction. Compared to the theoretical mechanical analysis which gives the tilt angle in z-direction of **0.109°** and the height change of the heated L-block of **172.62 μm**, the results from the FEA model are about twice as small. Even though an equal amount of heat was applied on the same surface area with the same air convection co-efficient, the mechanical analysis assumes a perfect heat transfer condition. Moreover, it only considers the expansion of the L-block in the z-direction and that the temperature throughout the L-blocks is uniform. These assumptions are responsible for the discrepancies in the mirror's tilt angle and the block's height change.

Rettner Setup FEA

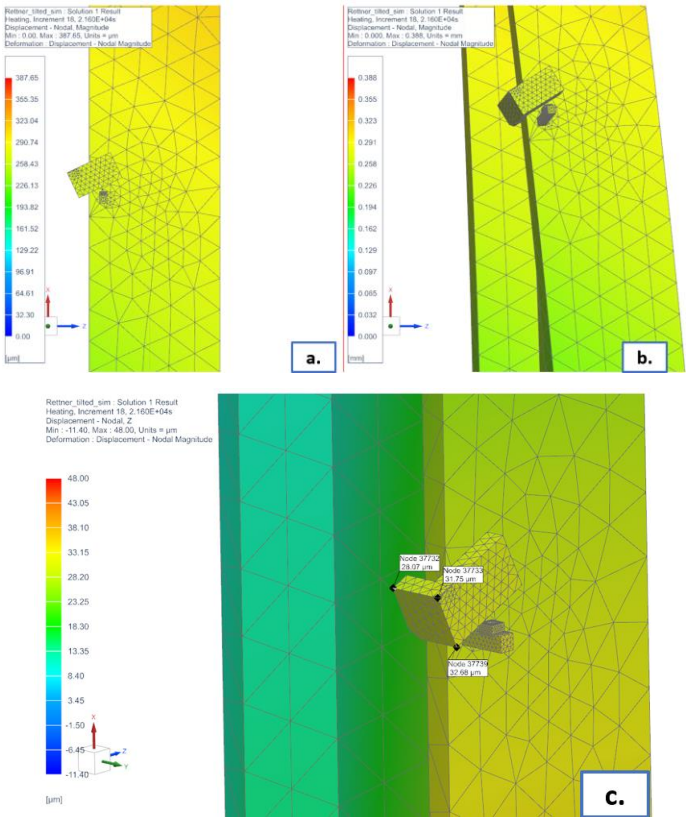

Figure 14: Displacement of the kinematic adapter due to heating of the steel beam in the Rettner setup FEA (NX): (a) total magnitude of displacement (b) total magnitude of displacement amplified 5000 times (c) displacement in the z-direction, used in the angle of tilt calculation

The Rettner setup was modeled with Siemens NX. A coupled structural-thermal FEA was performed on the setup to observe the impact Kapton heater heating has on the steel beam and to find the resulting tilt of the mirror attached to the beam. The thermal FEA assumed an applied thermal load of 33.3W and convective cooling by air with a heat transfer coefficient of $25\ \frac{W}{m^2 \cdot K}$. The rest of the loads and boundary conditions of the simulation can be found in Appendix V.

By using the displacement of three points on the front face of the adapter, where the mirror mount was attached, a plane was created, representing the newly tiled mirror. The angle between that plane and the original face of the mirror was found. The resulting angle of tilt of the mirror was found to be **0.00485°**. With the distance of 11.815m from the mirror to the camera detector, the magnitude of drift in Rettner setup calculated from FEA was **2.002 mm**. These FEA results will be used as the model for the Rettner experiment and will be compared to the experimental results.

MANUFACTURING

Kinematic adapter

In the optical mirror mount to steel beam adaptor (blue) design (Figure 15), there were several key factors in selecting the materials. Spherical magnets were selected to achieve strong quasi-kinematic contact. To control the magnet positioning, the adaptor needed to be non-magnetic as magnets were to be used to kinematically attach the mount to the beam. The adaptor also needed to have a low enough mass such that the magnets would support the mount and mirror. Additionally, it had to be rigid, and not deform due to ambient conditions. Therefore, aluminum 6061 was chosen as it meets all the previously mentioned conditions and is also easily accessible and easy to machine. The mount was manufactured using a mill as the design of the adapter consisted of straight edges, flat surfaces, and holes.

The holes on the mount were intended for steel alloy pins, which will hold the magnets at a designated position on the mount. A cold rolled steel rod with a diameter of 0.185 inches was chosen as the material of the pin because it was readily available at with the desired diameter to press fit the pins into the mount. A rotary tool with a cutting blade was used to cut the cold rolled steel rod because the rod was small in diameter and the equipment was readily available. The pins were ground-flattened using a vertical belt sander to ensure that the contact between the steel pins and the magnets are on a singular point. Then 2lb force, 3/8”-diameter neodymium magnetic spheres (orange) were attached to the steel pins and a combination of 45lb neodymium magnet blocks and a sphere were used to support the adapter from the bottom.

Table 5: Total Manufacturing Cost

COST	AMOUNT
Hardware	$ 40
Labor	$ 1050
TOTAL	**$ 1090**

If these parts were to be scaled to 1000 systems, the dimensions, such as thickness or length, of the adapter and the L-shaped blocks can be reduced to decrease the manufacturing time and cost of materials. This will reduce the overall manufacturing time and cost of manufacturing the component.

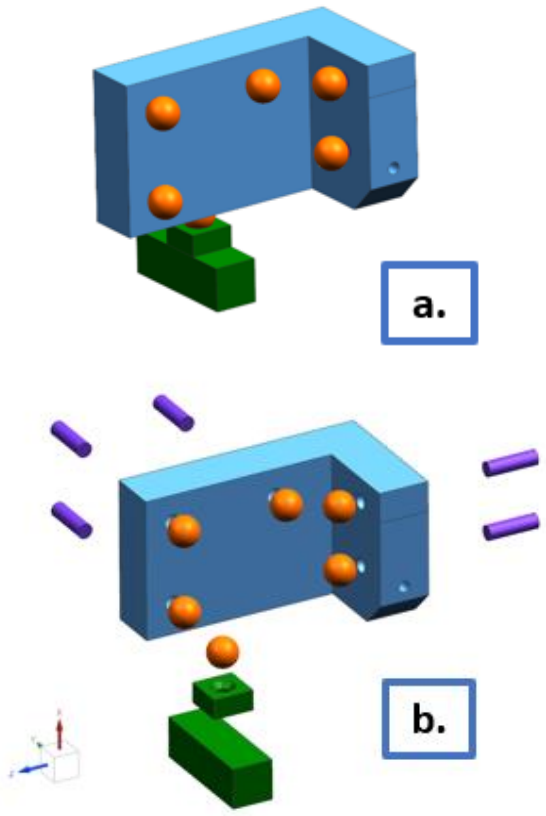

Figure 15: Adapter with steel pins and magnets CAD (NX) (a) assembled view (b) exploded view

Kinematic 3-stage plate

In the optical bench experiment, a kinematic 3-stage plate was designed and manufactured for a thermal experiment to investigate the association between the mirror and fringes' movement potentially caused by thermal source. The design includes a thin steel plate, three 3/8"-diameter spherical magnets, and three L-shaped aluminum blocks. The purpose is to have a mirror on an optical post attached to the thin steel plate supported kinematically by three aluminum L-blocks through three spherical magnet balls.

Since the heat was being applied directly on the L-blocks, the material needed to be highly thermally conductive. Together with the availability, aluminum was chosen to manufacture the L-blocks. The spherical magnets were purchased to achieve strong quasi-kinematic contacts. To have a surface that kinematically and magnetically contacts with the balls, the plate had to be magnetic and flat. Therefore, a thin, flat steel piece was chosen to be the plate. Small pivots were drilled under the plate for the magnetic balls to snap on the precise locations. Moreover, the spheres' material, neodymium (Nd), and the plate's material, steel, have significantly lower CTE which allows the aluminum L-block to be the only component expanding due to the heat. Kinematic contacts would therefore be more efficient. For the spherical magnets to stay kinematically in contact with the non-magnetic L-block, 0.625"-long and 3/16"-diameter steel pins were press fitted into the top surface of the L-block because it was readily available.

The aluminum L-blocks were manufactured using a vertical mill because they require a rough remove of materials. Moreover, the rectangular shape of the block required repeated translational and orthogonal cuts which made the vertical mill an efficient choice of manufacture. The vertical mill was also able to hold a large square plate well to drill the steel plate. A rotary tool with a cutting blade was used to cut the cold rolled steel rod because the rod was small in diameter and the equipment was readily available. The pins were ground-flattened using a vertical belt sander to ensure that the contact between the steel pins and the magnets are on a singular point. Finally, a press tool was used to press the steel pins into the holes on the L-block.

RESULTS & DISCUSSION

Table 6: Results of Specification tests

	Value	Unit	Description	Method of evaluation	Result
Specifi-cations	1	µm	The magnitude of drift caused by a thermal source	Simulations and Experiments	Passed
	0.1	°C	Maximum increase in ambient temperature due to measurement apparatus	Thermal camera	Failed

The first specification is to identify at least **1 μm** of drift caused by a thermal source through both simulations and experiments of the Rettner setup. With a heat source of 33.6 W applied over 8 hours overnight, the FEA simulation result shows a drift magnitude of **2.002 mm** while the experimental result shows **6.018 mm**. Therefore, the first specification of drift identified is achieved.

The second specification is to maintain the ambient temperature difference below or equal to **0.1°C**. The team failed to test and pass this specification since the Rettner experiment setup was removed without the team's knowledge before the relevant temperature data could be collected.

Thermal LLE FEA

The theoretical drift values computed through the rotation values that were obtained through the thermal FEA suggest that a tiny change in the thermal profile in the structure can lead to drift in the laser. The largest drift magnitude computed with the rotation values from the thermal FEA was at transport mirror 30. From the LLE's ultraviolet stability test (appendix I), Transport mirror 30 has the 7th largest average drift and 5th largest median drift out of 60 transport mirrors.

The drift value deduced from the FEA was **16.917µm** with **0.98%** error compared to the drift value of **mirror 30** from appendix I, 17.092µm. However, the drift values of all the other mirrors had over 33% error compared to the LLE's stability data. This indicates that there are more sources of heat that were not captured or there are other sources that cause the affect the drifting behavior of the laser.

Optical Bench Setup

Two experiments were run on an optical bench with 40V heating. Each experiment was divided into separate heating and cooling videos. The resulting plots are found in figures 16 to 19. In figure 16, a gradual change in both fringes spacing, and angle is seen in the April 11th experiment, which levels off after approximately 8 minutes of heating. As the setup cools in figure 17, the opposite change is seen as the fringes return to their initial position.

The results from April 9th in figures 18 and 19 follow a similar fringe spacing trend as the April 11th experiment. However, angle seems to be experiencing erroneous fluctuations which may be caused by noise in the data due to too much ambient light or human presence in the room such as walking. Further experiments would be expected to follow comparable results as the April 11th experiment since thermal expansion due to constant heating would follow an exponential curve as shown.

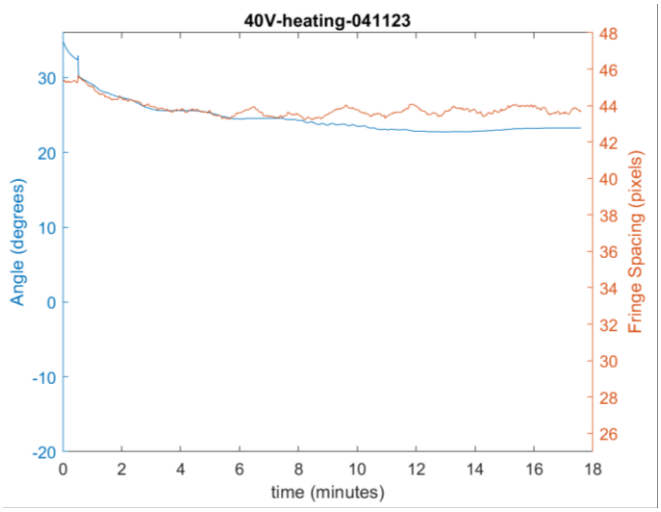

Figure 16: Optical bench 40V heating on April 11th, 2023

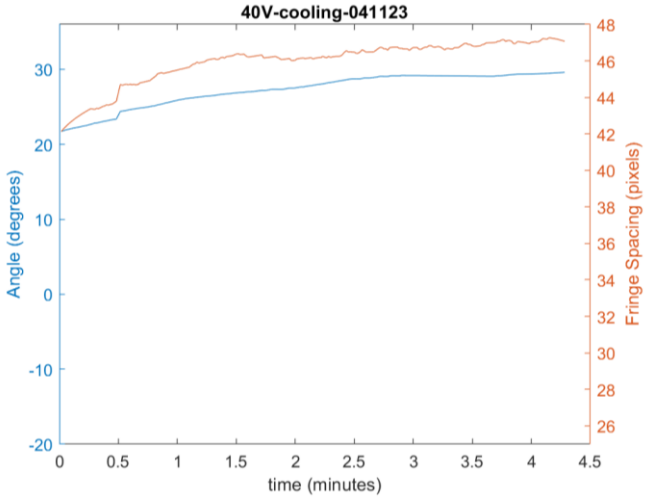

Figure 17: Optical bench 40V cooling April 11th, 2023

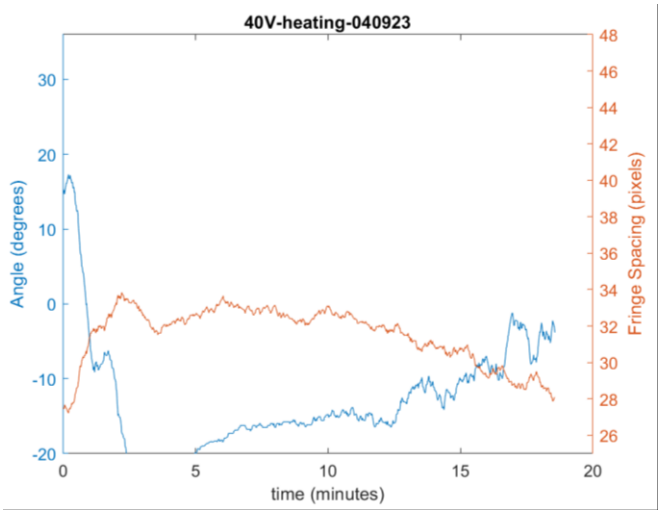

Figure 18: Optical bench 40V heating on April 9th, 2023

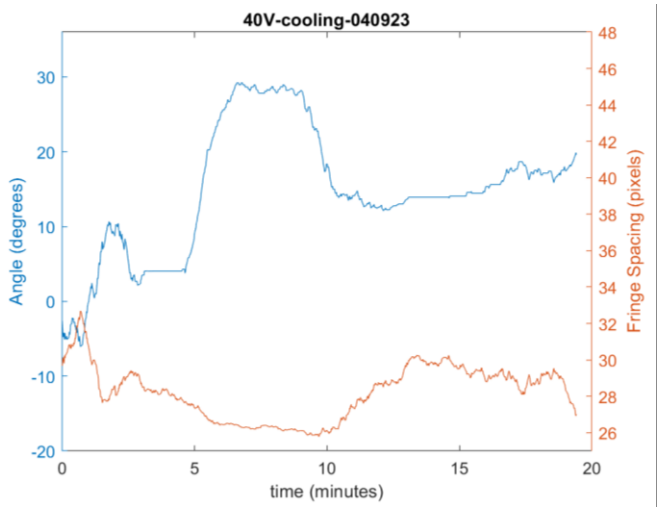

Figure 19: Optical bench 40V cooling on April 9th, 2023

Table 7: Fringe angle and spacing results of Optical bench experiment

Heat source 40V – 16.08W		Fringe spacing [px]		Fringe angle [°]	
		Λ_1	Λ_2	ϕ_1	ϕ_2
April 9th	Heating	Error			
	Cooling				
April 11th	Heating	45.3	43.7	34.3	23.3
	Cooling	42.5	47.1	22.0	29.6

Table 7 shows the results of the fringe angle and fringe spacing at the beginning and ending of each 20-minute heating and cooling cycle. As discussed, the recorded data for the April 9th experiment is unreliable. For the April 11th experiment, the results are reasonable since the drift occurred due to thermal sources increased as heated and decreased as cooled. The changes in fringe spacing and fringe angle when heating and cooling were comparable, as also demonstrated visually in Figure 16 and 17. Using Equation (15)-(20), the drift results of the April 11th experiment are,

Table 8: Drift results of Optical bench experiment on April 11th

Heat source 40V – 16.08W	d_x [mm]	d_y [mm]	d_{total} [mm]
Heating	0.475	-0.0007	**0.475**
Cooling	-0.573	-0.0004	**0.573**

From the calculated drifts and the behavior of the fringe movement, it is convinced that the mirror moved as one L-block was heated and returned to the approximate original position when the block was cooled. The **FEA results** of the optical bench setup output the tilt angle of 0.0564° which correspond to **0.750 mm** of total drift. Compared the total drift from the experimental heating and cooling results with that from the FEA, there are errors of **-36.7%** and **-23.6%**.

Rettner Setup

The resulting fringe analysis yields Fringe Angle and Fringe Spacing for each frame of the video. The Fringe Angle and Fringe Spacing plots can be found in figure 20 along with Angle Norm, which represents the Angle data normalized to an initial angle of 0 degrees.

Table 9: Fringe angle and spacing results of Rettner experiment

Heat source	Fringe spacing [px]		Fringe angle [°]	
	Λ_1	Λ_2	ϕ_1	ϕ_2
10V – 4.10W	69.8	71.1	4.2	5.9
20V – 33.6W	72.9	67.3	0.6	1.5

Table 9 shows the results of the fringe angle and fringe spacing at the beginning of heating and at 6-8 hours after were generated by the MATLAB code. Using Equation (14)-(19), the drift results are,

Table 10: Drift results of Rettner experiment

Heat source	d_x [mm]	d_y [mm]	d_{total} [mm]
10V – 4.10W	-1.577	-0.0003	**1.577**
20V – 33.6W	6.018	0.001	**6.018**

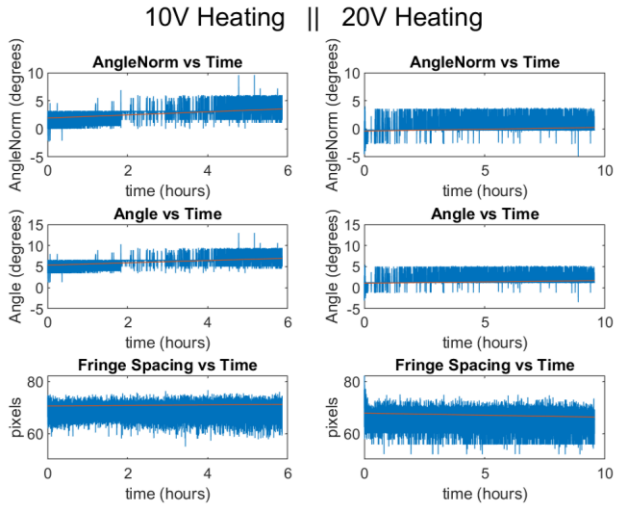

Figure 20: Data collected from the 10V and 20V Rettner heating experiments over 6 and 10 hours, respectively.

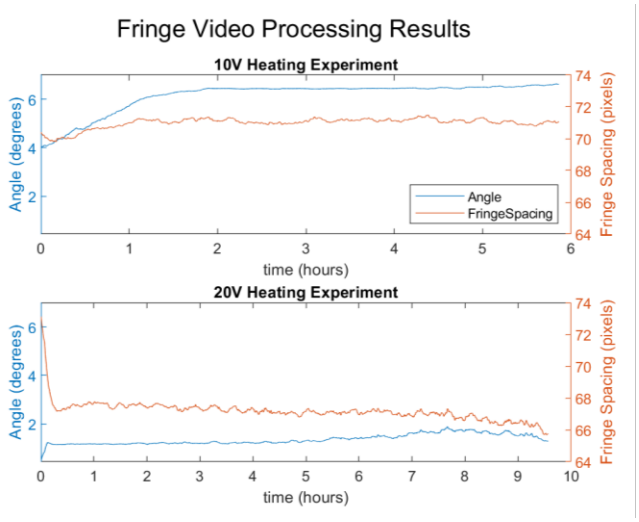

Figure 21: Results of fringe video processing from the 10V and 20V Rettner heating experiments over 6 and 10 hours respectively

Compared to the **FEA** drift result of **2.002 mm** for a **20V**-33.6W heating setup, the experimental result of **6.018 mm** is about three times larger.

LLE Cal-out Data Analysis

During 11 days in 2020 and 2021, the LLE took drift data of all 60 OMEGA-60 beams. The raw data of each mirror's drift in the x and y direction was given over to the team. That data was analyzed and sorted using Microsoft Excel (Annex I) to look for trends in drift between different beams. Each beam was assigned

a drift rank, based on its average and median drift over the 11 days, 1 being the highest drift and 60 being the lowest. Median is the more accurate parameter, as outliers from a single day were skewing the mean significantly.

The beams were also organized into "families" (groups of 2-6 beams) based on the location of the target mirrors, that reflect those beams, on the north/south end structures (i.e., mirrors located in the lower east of the north and structure were placed in the "North Lower East" family). The trends between different families and inside the same family were analyzed using the CAD of the north/south end structures and the sorted drift data.

The common trend that stood out the most between beam drift was that beams reflected from mirrors pointed down tended to have larger drift. Following that, a statistical calculation was performed to determine the reliability of this observation. The calculation was done through a two sample Z-test with proportions Appendix VII. The calculation concluded that downward facing mirrors are **13%** more likely to experience above median drift (at 95% significance level).

Since the main hypothesis is that stray thermal sources cause deformations in the structure that lead to drift, mirror families can be particularly interesting due to their proximity to each other. The 4-mirror family "NLE" contains the 4th and 5th worst mirrors along with the 40th and 44th worst. With only 60 mirrors this is a drastic variation across mirrors that should share similar temperature profiles and drift behavior. Other examples of this family variation can be found in table #. The "SLE" family variation agrees with the downward pointing mirror hypothesis since both high drift mirrors point downwards while both upward pointing is low drift. However, the "NLE" family seems to be indifferent to mirror orientation as it has examples of downward and upward facing mirrors each exhibiting both high and low drift.

Many mirrors share steel mounting plates but have large variations in drift. Mirrors 62 and 63 share a plate and have the 1st and 37th highest drifts, respectively. This discrepancy may be explained by orientation as beam 62's mirror points downward whereas mirror 63's mirror points upwards. Similar behavior is seen in mirror 57 and 58 who share a plate, have high drift discrepancy, and have differing orientations. Mirrors 20 and 29 also demonstrate this upward/downward discrepancy on a shared plate. Mirrors 32, 33, 34, and 35 share a plate and all point upward yet 34 and 32 show low drift, 35 shows high drift, and 33 shows moderate drift. In the absence of varying orientations, it is unclear what could be causing this variation. It is expected that mirrors on a shared plate would drift similarly when displaced by thermal expansion of the structure as our main hypothesis states. The shared plate mirrors 36, 37, 38, and 39 show behavior that contradicts the mirror orientation hypothesis: the high drift mirrors are pointing upwards and the low drift mirrors are pointing downwards.

Table 11: Mirror families with large variations in drift

Family	Member Median Drift Ranks (lower is worse drift)
NLE	4, 5, 40 ,44
NLME	8, 58
NUW	11, 53, 54, 56, 57, 59
SLE	13, 19 38, 52
SUE	7, 20, 21, 22, 26, 50
SUM	2, 9, 10, 12, 34, 48
SUW	1, 6, 14, 17, 37, 43

INTELLECTUAL PROPERTY

The design of the kinematic adapter was found to be patentable. The closest design found was a THORLABS Kinematic Base [6]. The product mechanism is to use two plates to mount an object onto the base and mount the base onto an object through kinematic and magnetic contacts. If this design were applied in the Rettner setup, one plate would be mounted onto the steel beam and the other one would hold the mirror. However, this would require the steel I-beam in Rettner to be drilled, which damages the building facility. The team's design of six kinematic and magnetic points of contact created by using spherical magnets that connect directly to the beam avoids this issue. Therefore, the design is unique enough to be considered patentable.

SOCIETAL AND ENVIRONMENTAL IMPLICATIONS

Fusion power, often hailed as a clean and sustainable energy source, can significantly reduce the environmental impacts associated with traditional energy production. Fusion produces energy with minimal greenhouse gas emissions and generates only insignificant amounts of low-level radioactive waste. Unlike fission-based nuclear power, fusion does not pose the risk of catastrophic accidents, as the reaction terminates if conditions become unstable. This project is aimed to help nuclear fusion research and contribute to the goal of making fusion powerplants a reality.

RECOMMENDATIONS FOR FUTURE WORK

The thermal FEA performed on the full transport mirror structure had thermal loads directly loaded onto the beams themselves. However, the heat is radiated from a heat source sitting close to the structure or conducted through a medium to heat up the structure. Therefore, a more accurate model can be performed by having heat sources radiate or conduct heat to the transport mirror structure. Also, there were areas that were not accessible to go into to take thermal images of all the mirrors. It

would be extremely beneficial if thermal images of all the transport mirrors and their surrounding environments could be acquired for more precise simulation.

From the thermal images that was taken inside the target bay of the Omega-60 Laser system, it was found that the highest temperature profile was observed on the motors that are on the mirror mount, which are used to hold the mirror at specific angular orientations. For future work, a thermal analysis of the mirror mount on the LLE transport mirror structure can be performed to see if the motors affect the position of the mirror. Also, a sample transport mirror mount obtained from the LLE can be connected to the power source with a control system to actuate the motors and observe the temperature profile changes in the motors using the thermal camera. It is hypothesized by the team that mirrors pointed downwards are associated with increased actuator temperatures and higher drift. If this is true, self-locking power screws may present an alternative to actuators more resistant to orientation.

In addition, there seems to be a relation between the mirror's orientation and the drift's magnitude, discovered through analysis of the ultraviolet drift data provided by LLE. It was observed that the mirrors that were tilted downwards tend to have a higher drift. This can be verified using having the mirror mount sit at a varying angle and using the Mach-Zehnder Interferometer, like was used in the Rettner setup, to observe the movement of fringes over extended periods of time.

For further exploration of beam heating experiments, it is suggested that a quad cell setup be used instead of the interferometer one. Interferometer calculations are complex and fringe data is difficult to analyze accurately. In theory, quad cells are much easier to gather data from and the calculations are not as difficult either. The biggest issue would be acquiring a quad cell with a strong enough resolution to measure micron level drift, though many could be found to fit in a $1000 budget of the project.

Also, multiple runs of 24-hour experiments might be beneficial, as temperature fluctuations of the building throughout a full day might have a significant effect on the drift. Also runs of long heating and cooling, to see if drift returns to its original position after cooling.

For further analysis of LLE drift data, it was noticed that mirrors located on diagonal support beams tend to have higher beam drift, however not enough data is provided to make any concrete conclusions. The accuracy of the analysis would increase dramatically if data over more days is provided. 11 days is not enough to locate accurate drift trends correlations between beams.

ACKNOWLEDGMENTS

We acknowledge our instructors, Professor Christopher Muir and Professor Edward Herger, our sponsor, Professor Ethan Burnham-fay, and our teaching assistant, Robert Nowak, for their guidance in problem definition, design, and experiment concepts, and building the experiments. We also appreciate the manufacturing advice and equipment provided by Jim Alkins and Christine Pratt. We would also like to thank the Laboratory for Laser Energetics (LLE) for letting us visit the target bay to collect thermal images on-site, Albert Consentino for the safety training, and Jeff Hart for the escort of the visit. Our team also thank Charles Fleischmann for the suggestions about the self-locking power screws mechanism as a potential improvement for the mirror mount used at LLE and Riya Sharma for the detailed peer review.

REFERENCES

[1] “Omega Laser Facility.” Laboratory for Laser Energetics, June 16, 2021. https://www.lle.rochester.edu/index.php/omega-laser-facility-2/.

[2] Aharon, Oren. "Laser Autocollimator and Bore Sighting." Novuslight. July 21, 2014. https://www.novuslight.com/autocollimator-laser-and-bore-sighting_N2822.html.

[3] “Position Sensing Detectors.” Thorlabs, Inc. - Your Source for Fiber Optics, Laser Diodes, Optical Instrumentation and Polarization Measurement & Control. Accessed April 26, 2023. ww.thorlabs.com/newgrouppage9.cfm?objectgroup_id=4400.

[4] LIGO Laboratory. “What Is an Interferometer?” Laser Interferometer Gravitational-Wave Observatory. Caltech. Accessed April 26, 2023. https://www.ligo.caltech.edu/page/what-is-interferometer#:~:text=Interferometers%20are%20investigative%20tools%20used,%2Dmeter'%2C%20or%20interferometer.

[5] “Inclinometer Specifications.” Posital. Accessed February 19, 2023. https://www.posital.com/en/products/inclinometers/mems/MEMS-Technology.php

[6] “Kinematic Bases” Thorlabs, Inc. - Your Source for Fiber Optics, Laser Diodes, Optical Instrumentation and Polarization Measurement & Control. Accessed April 26, 2023 https://www.thorlabs.com/newgrouppage9.cfm?objectgroup_id=1546

APPENDIX I: Drift Data Analysis

Table 12: Drift data collected from LLE and analyzed by team

Beam	avg dx	median dr	avg dr	Avg Drift Rank	Med Drift Rank	Angle from + Z axis (degrees)
25	-0.206	12.029	20.098	1	31	96.0549498
35	1.081	17.364	19.024	2	4	76.98053693
62	0.841	21.017	18.591	3	1	102.0431024
54	1.295	14.641	17.712	4	16	98.68753769
50	4.733	18.315	17.560	5	3	92.4866646
37	0.637	12.471	17.277	6	27	82.43268595
30	2.018	17.085	17.169	7	5	97.62447722
69	4.975	10.800	17.145	8	39	90.63606085
29	-3.418	15.781	17.002	9	8	98.68984794
42	-1.476	15.829	16.529	10	7	93.41185994
66	-6.230	15.020	16.483	11	14	83.48813762
57	3.013	18.611	16.245	12	2	98.76528027
45	-2.755	15.049	16.114	13	13	99.61404887
36	8.186	11.919	15.929	14	32	86.54120709
38	-1.457	9.454	15.918	15	49	99.76849423
48	4.009	13.624	15.601	16	21	65.67466073
12	-4.279	15.176	15.536	17	11	102.8372849
44	-0.093	14.016	15.518	18	19	93.66050288
56	-3.043	15.335	15.374	19	9	74.51427073
43	1.686	13.256	15.287	20	22	102.6978379
52	3.260	15.156	15.264	21	12	72.94833441
21	-1.218	12.689	14.739	22	24	106.1330188
51	1.845	15.243	14.495	23	10	107.2120683
68	-1.320	16.915	14.156	24	6	74.22490405
34	2.830	10.316	14.062	25	44	77.24749674
26	4.255	10.422	13.754	26	42	74.44273303
19	1.724	12.460	13.690	27	28	100.0788327
22	-5.301	14.080	13.690	28	18	71.99978205
59	-1.727	14.709	13.621	29	15	80.04974479
14	3.048	12.186	13.571	30	30	91.83411175
27	8.128	12.290	13.170	31	29	91.88825889
67	3.293	14.181	13.036	32	17	90.70566527
33	5.583	12.953	12.939	33	23	63.29723723
46	-0.661	12.485	12.777	34	26	69.50918403
16	7.025	8.800	12.620	35	54	97.23059629
28	2.255	12.586	12.530	36	25	68.65110503
39	2.975	10.794	12.325	37	40	91.27418921
63	3.366	11.143	12.150	38	37	87.3320982

24	2.927	11.194	12.093	39	36	80.04908315
47	-5.472	9.049	12.076	40	50	86.22103053
31	-1.661	11.866	11.980	41	33	70.38474531
23	4.019	9.561	11.978	42	47	95.70486669
40	2.351	11.082	11.917	43	38	69.91703463
55	-0.605	11.208	11.867	44	35	58.37510019
60	8.365	10.515	11.656	45	41	72.78084303
65	-3.022	9.919	11.477	46	45	67.38284804
15	4.796	6.143	11.355	47	60	74.40819941
32	6.615	9.703	10.923	48	46	84.55063816
61	-1.905	10.402	10.921	49	43	74.56876179
53	1.387	11.296	10.582	50	34	88.47784646
41	-1.192	13.654	10.405	51	20	89.84056988
10	3.643	9.011	10.387	52	51	68.78655766
49	1.418	8.888	9.994	53	52	80.27895114
58	-0.472	9.543	9.802	54	48	75.39585626
64	-0.894	7.792	9.403	55	55	98.61564984
11	0.378	8.800	8.804	56	53	80.52416718
13	3.920	7.550	8.620	57	57	79.857481
17	1.096	7.615	8.592	58	56	72.3490163
20	-1.795	6.886	8.577	59	58	67.29330018
18	5.669	6.516	8.355	60	59	89.52294481

APPENDIX II: Boundary Conditions for LLE Transport Mirror Structure Thermal FEA and Nodal X, Y, Z Displacements

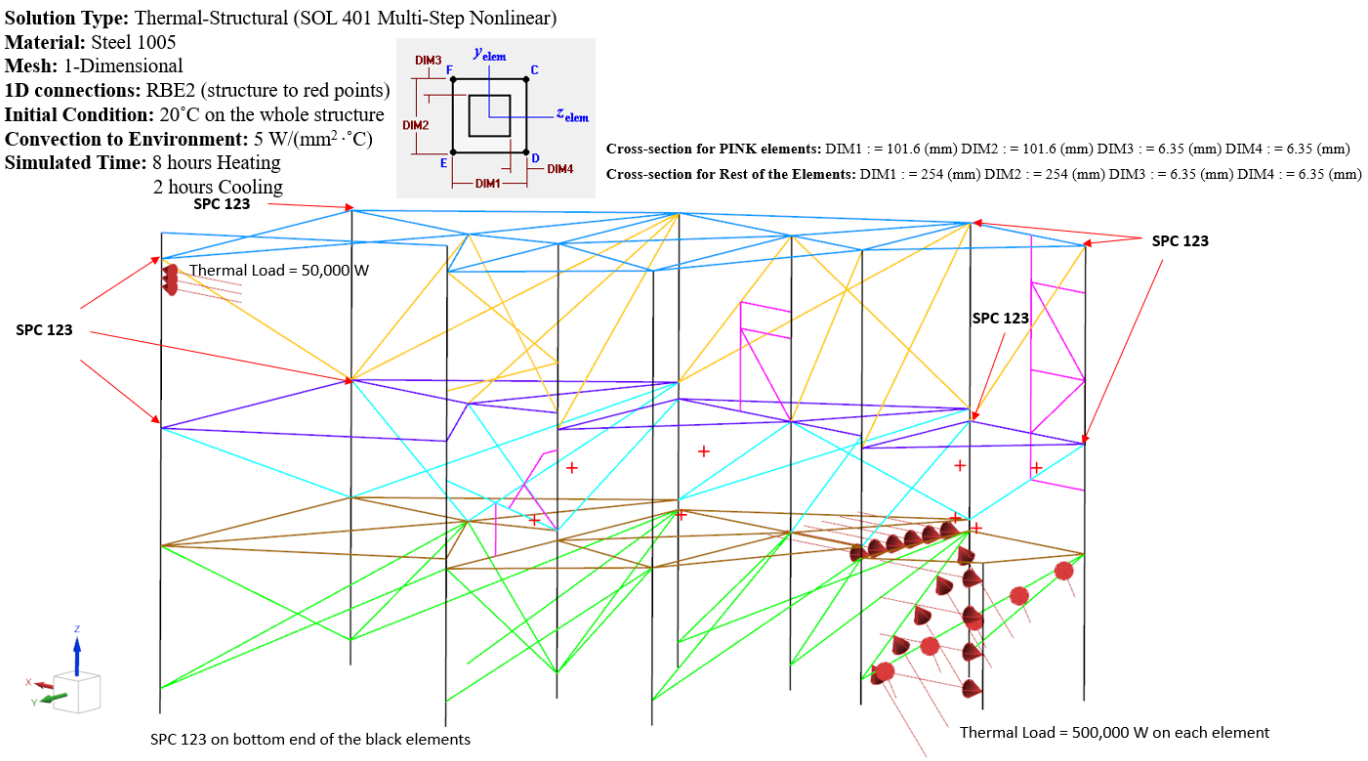

Figure 22: Boundary Conditions of LLE Transport Mirror Structure Thermal FEA

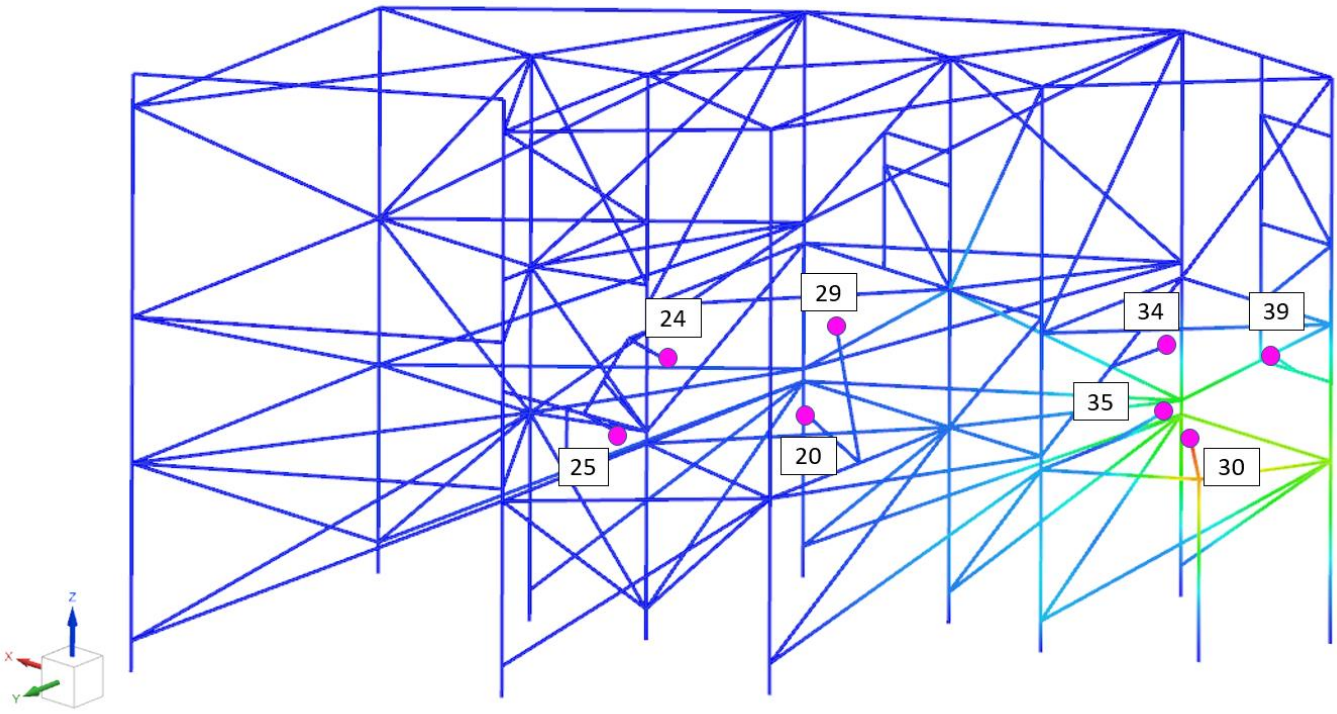

Figure 23: Magnitude of overall Displacement in the Transport Mirror Structure due to Heat Sources with 8 magenta circles that represents the center point of the transport mirrors numbers corresponds to the mirror ID number

Table 13: Transport Mirror Displacement [μm]

Mirror ID	X	Y	Z	Magnitude
24	-0.08529	-0.00401	0.03087	0.09079
25	-0.1016	-0.01772	0.01508	0.1042
29	-0.3155	-0.2353	-0.1038	0.407
20	-0.272	-0.2027	-0.08523	0.3498
30	0.9499	-2.452	2.221	3.442
39	0.3372	-0.9972	-0.356	1.111
34	-0.17	-0.06742	-0.09714	0.2071
35	0.1517	-1.049	0.09761	1.064

APPENDIX III: Thermal Images of the Heat Sources

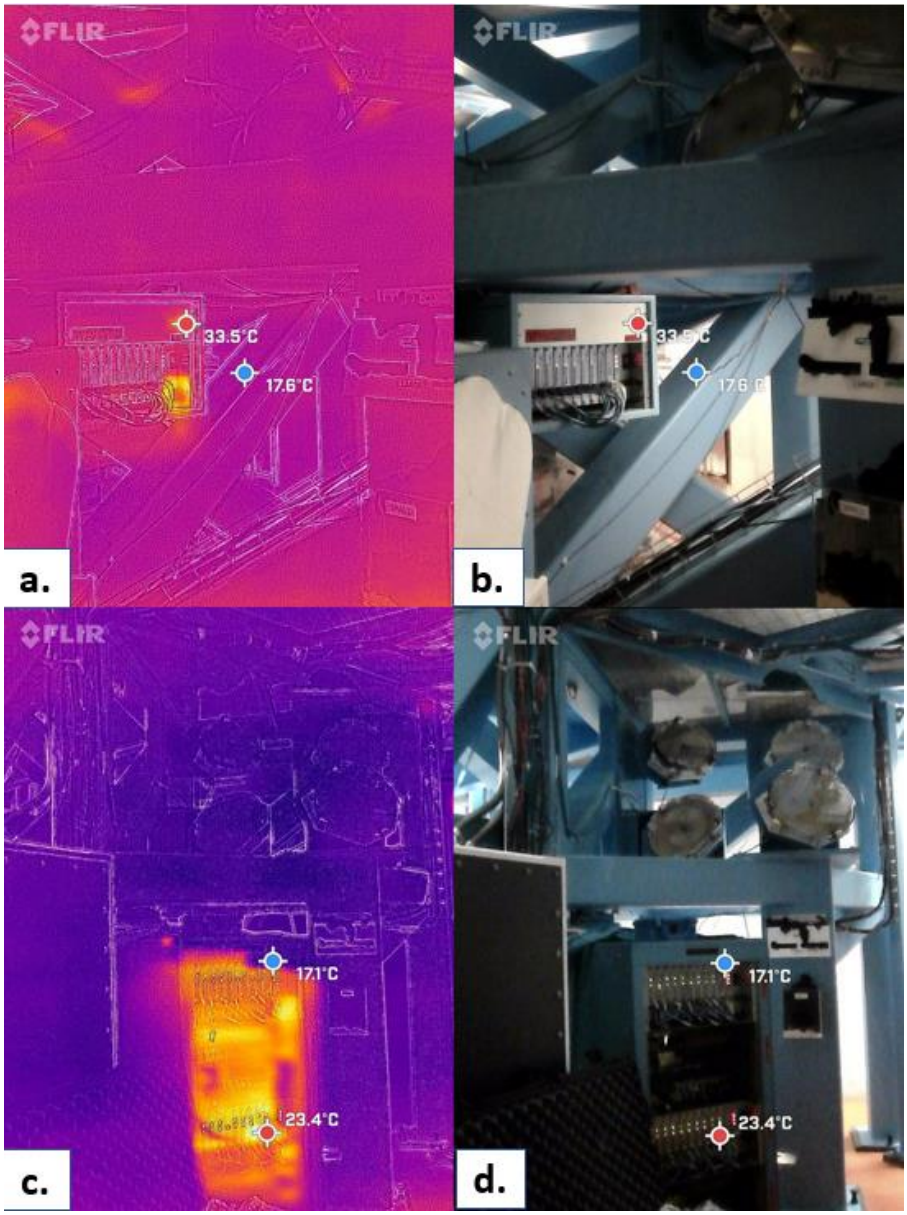

Figure 24: Thermal images of localized heat sources at bottom right of LLE Transport Mirror Structure taken by FLIR camera (Left: Thermal profile, right: Real image)

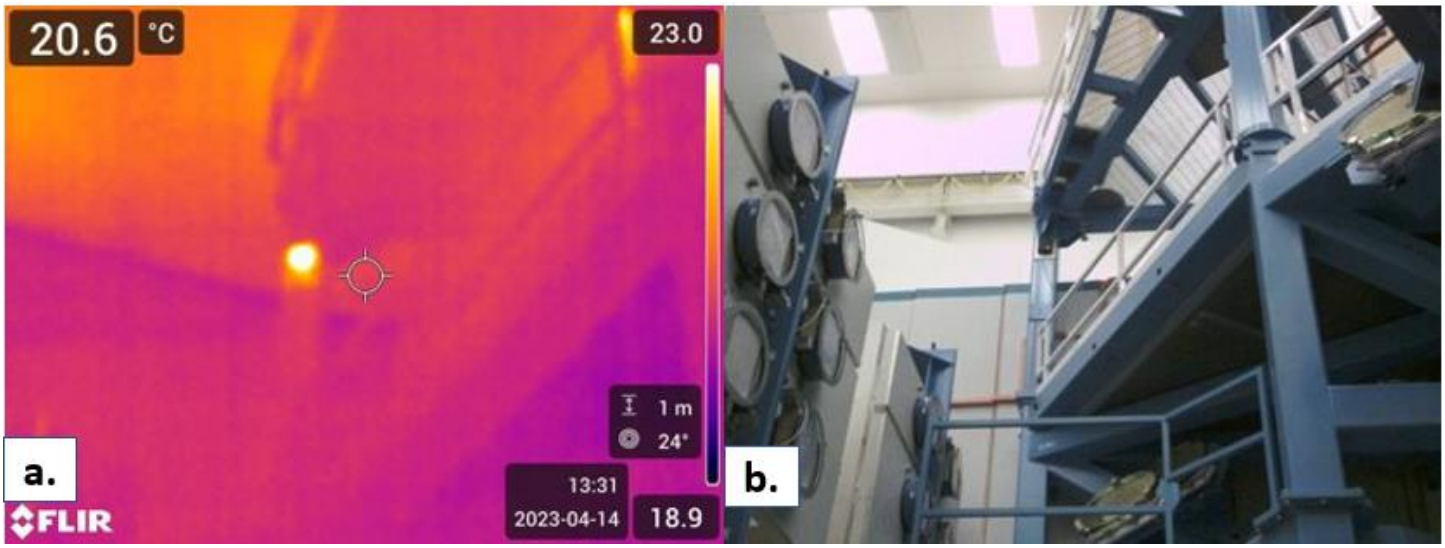

Figure 25: (a) Thermal image, (b) Real image of localized heat source at upper left of LLE Transport Mirror Structure taken by FLIR camera

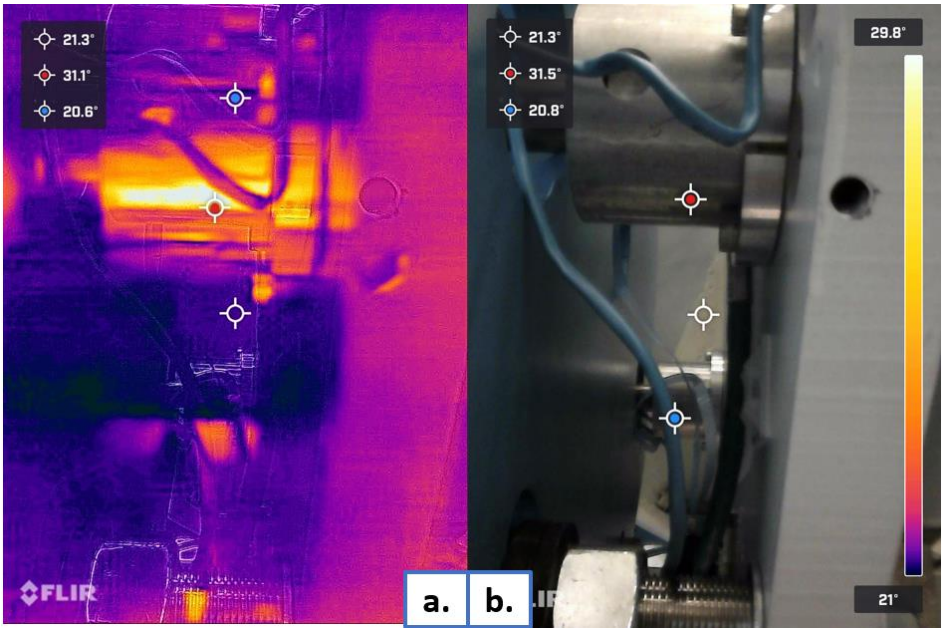

Figure 26: (a) Thermal image, (b) Real image of motors on back of mirror mount. Temperatures reach 31 degrees Celcius

APPENDIX IV: Optical Bench Experiment Thermal FEA

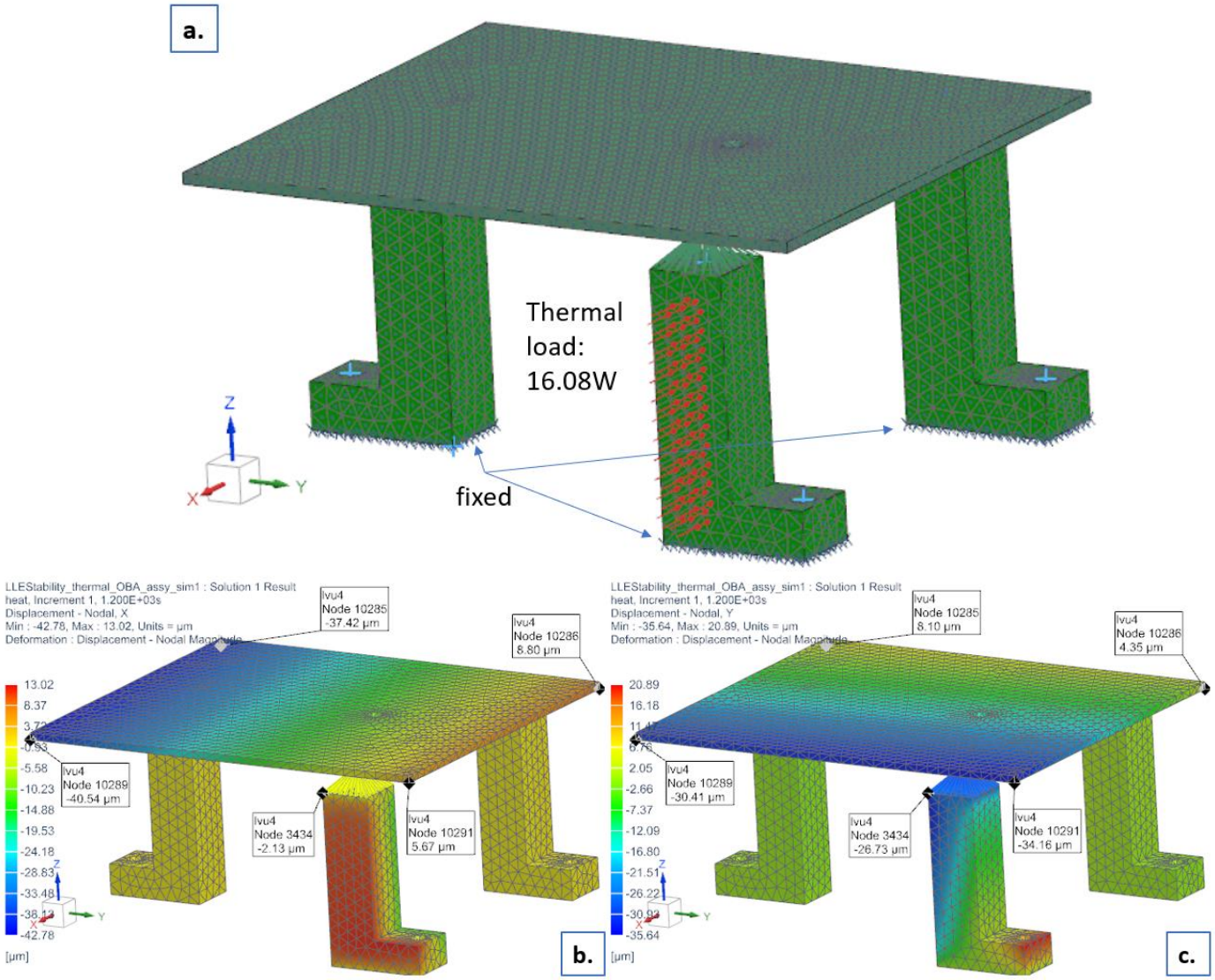

Figure 27: (a) Boundary conditions, (b) (c) Displacements of locations of interests in X and Y of the Kinematic 3-stage platform Thermal FEA

APPENDIX V: Boundary Conditions for Rettner Experiment Thermal FEA

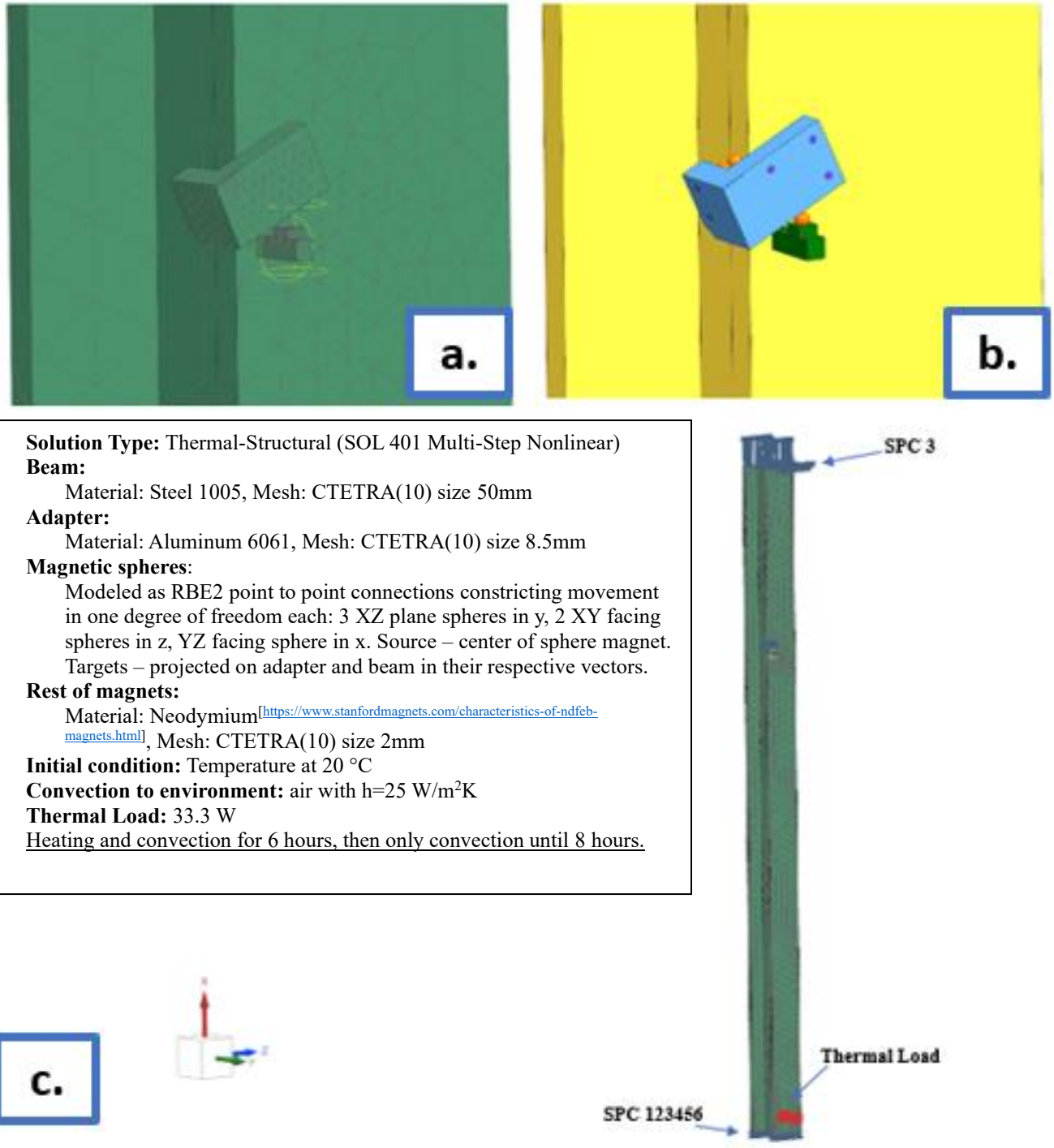

Solution Type: Thermal-Structural (SOL 401 Multi-Step Nonlinear)
Beam:
Material: Steel 1005, Mesh: CTETRA(10) size 50mm
Adapter:
Material: Aluminum 6061, Mesh: CTETRA(10) size 8.5mm
Magnetic spheres:
Modeled as RBE2 point to point connections constricting movement in one degree of freedom each: 3 XZ plane spheres in y, 2 XY facing spheres in z, YZ facing sphere in x. Source – center of sphere magnet. Targets – projected on adapter and beam in their respective vectors.
Rest of magnets:
Material: Neodymium[https://www.stanfordmagnets.com/characteristics-of-ndfeb-magnets.html], Mesh: CTETRA(10) size 2mm
Initial condition: Temperature at 20 °C
Convection to environment: air with h=25 W/m^{2}K
Thermal Load: 33.3 W
Heating and convection for 6 hours, then only convection until 8 hours.

Figure 28: Rettner setup (a) FEM of kinematic mount (close), (b) CAD of kinematic mount (close), (c) Loads and constrains of simulation, FEM details

APPENDIX VI: Fringe-Associated Drift Calculation

Nanometer-Pixel Conversion through Mechanical Adjustment experiment

In this experiment, the nob of a mirror is adjusted mechanically to associate the known mirror's tilt angles to the movement of fringes. Due to the nature of the interferometer set up in Rettner hall, it is more achievable to mechanically adjust the nob of the fixed mirror instead of the moving one. Since there is no thermal load on the beam that the moving mirror is mounted on, the moving mirror is now acting fixed.

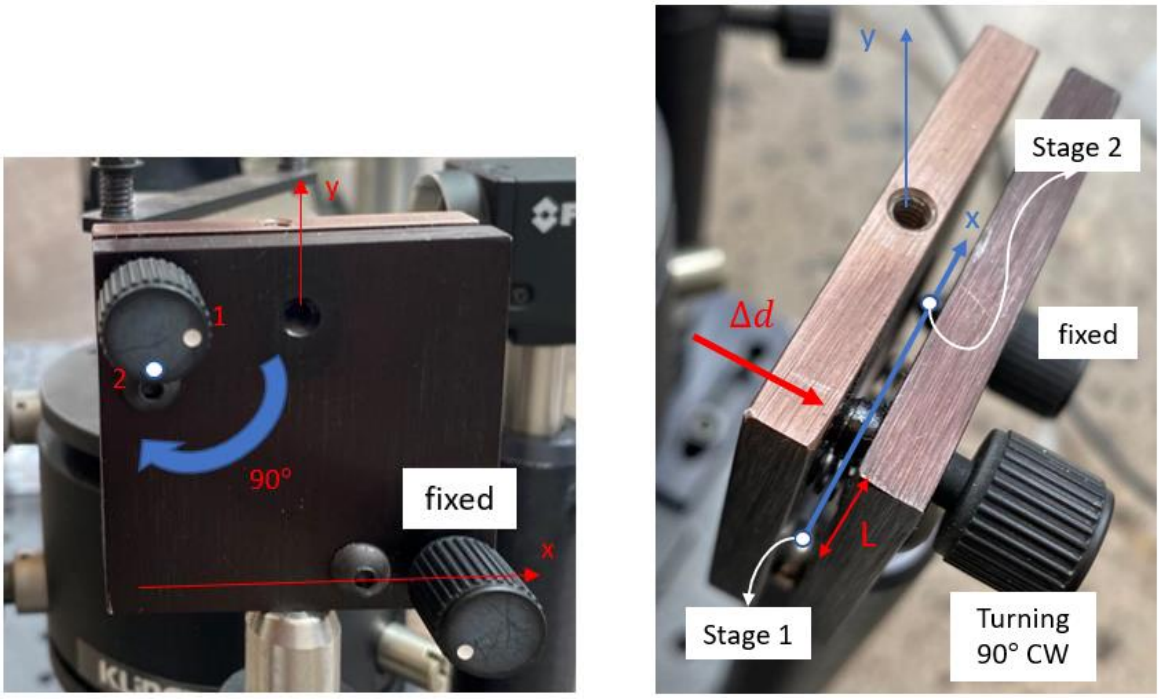

Figure 29 – (a) Mechanical adjustment of the mirror nob, (b) Tilt angle analysis of mirror around x-axis

As Figure 29a shows, the upper left mirror nob is being turned 90° clockwise from position 1 to position 2. This process was repeated over one minute to make sure the fringe movement is repetitive and the angle and fringe spacing corresponding to each nob position can be averaged. Figure 29b shows how the rotation of the mirror nob relates to its screw's translational displacement, and therefore, the change of tilt angle of the mirror around the x-axis (made of a line connecting the two other stages).

The mirror nob's screw has 100 threads per inch (TPI = 100). Hence, the minimum incremental movement (MIM) is calculated to be,

$$MIM = \frac{1/TPI}{360°} \tag{21}$$

Since the rotation made is -90° (clockwise), the translational displacement of the nob, Δd, is calculated to be -2.50E-3 [in] using Equation (8).

$$\Delta d = MIM \cdot -90° \tag{22}$$

$$\Delta\theta_x = \tan^{-1}\frac{\Delta d}{L} \tag{23}$$

The change of tilt angle of the mirror around the x-axis, $\Delta\theta_x$, is then determined to be -0.0015995 [rad]. This change of mirror angle around the x-axis will also be calculated in terms of [px] using the fringe movement analysis. From there, a standardized nanometer-pixel conversion will be determined.

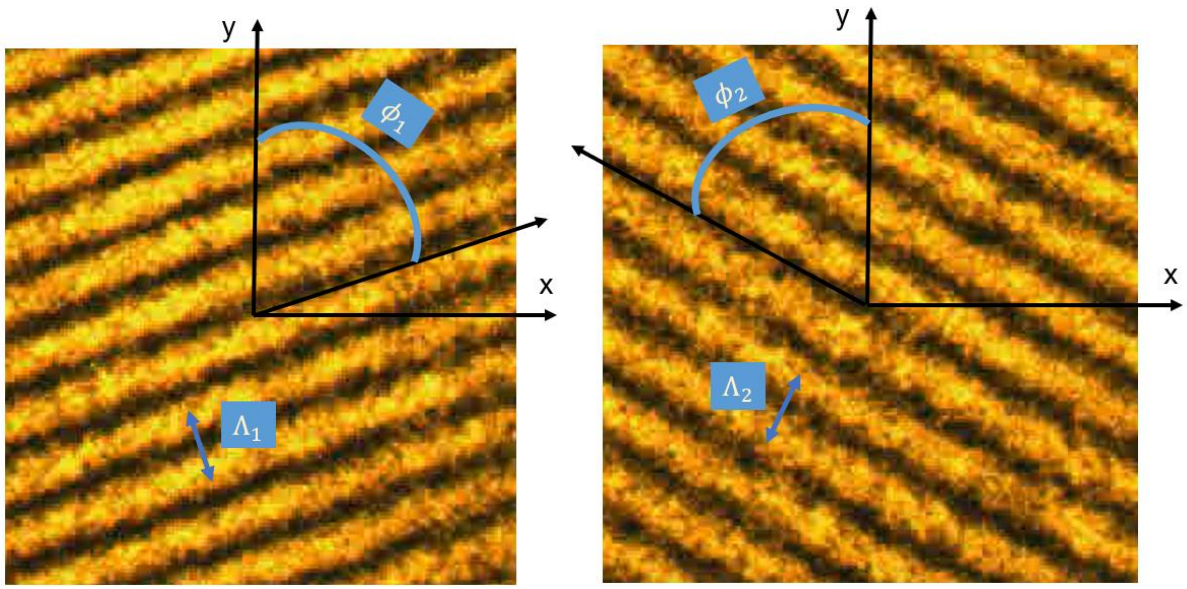

Figure 30 – Fringe movement of mechanical adjustment experiment: (a) Fringe position when the mirror nob is at position 1, (b) Fringe position when the mirror nob is at position 2. * *Refer to Figure 29 for the mirror nob adjustment diagram*

Similar to the fringe calculation discussed above in the heating experiment, the parameters given for each fringe image are the fringe spacing and the fringe angle: Λ_1 = 30.5 [px], Λ_2 = 111 [px], ϕ_1 = 69.20°, ϕ_2 = -60.02°. Note that even though the value of the fringe spacings of the second image is almost 4 times larger than that of the first image, they visually seem not too different from each other. This is due to the fact that during the rotation, the fringe spacing increases from 30.5 [px] to 73.5 [px] and then goes back to 35.5 [px] as it rotates through the vertical position. Therefore, fringe spacing accounts for the total change rather than just the net value of the displacement.

Using Equation (15)-(20), the tilt angles of the mirrors correspond to each mirror nob position are: θ_{x_1} = 3.68 [nm/px], θ_{y_1} = 9.70 [nm/px], θ_{x_2} = 1.42 [nm/px], θ_{y_2} = 2.47 [nm/px]. The angle change around the x-axis is calculated as,

$$\Delta\theta_x = \theta_{x_2} - \theta_{x_1} \tag{24}$$

Using Equation (10), the fringe position data provides that $\Delta\theta_x$ = -2.26 [nm/px], while the mirror nob displacement calculation indicates that $\Delta\theta_x$ = -0.0015995 [rad] or [nm/nm]. These two values are equal, leading to a conversion of,

$$\frac{-2.26\ [^{nm}/_{px}]}{-0.0015995\ [^{nm}/_{nm}]} = 1413.04\left[\frac{nm}{px}\right] \tag{25}$$

In addition, the angle change around the y-axis is expected to be zero since no mechanical adjustment is made around the y-axis. In reality, the angle change around y-axis is non-zero. Sources of errors can possibly come from the imprecise manual adjustment of the mirror nob, unexpected sources of vibration occurring on the fixed mirror mounted on the beam, or the fringe rotation tracking MATLAB code.

APPENDIX VII: Two Sample Z-test with Proportions

$$H_0: p_1 - p_2 = c \tag{26}$$

$$H_a: p_1 - p_2 \neq c \tag{27}$$

Where p_1 is the probability that a downward facing mirror has above median drift and p_2 is the probability that an upward facing mirror has above median drift.

$$\alpha = 0.05$$

For the first iteration c = 0.

$n_1 = 24$ (Number of mirrors tilted down) $x_1 = 17$ (number of tilted down mirrors with above median drift)

$n_2 = 36$ (Number of mirrors tilted up) $x_2 = 13$ (number of tilted up mirrors with above median drift)

$$\hat{p}_1 = \frac{x_1}{n_1} \tag{28}$$

$$\hat{p}_2 = \frac{x_2}{n_2} \tag{29}$$

$$\hat{p} = \frac{x_1 + x_2}{n_1 + n_2} \tag{30}$$

$$Z = \frac{(\hat{p}_1 - \hat{p}_2) - c}{\sqrt{\hat{p}(1-\hat{p})\left(\frac{1}{n_1} + \frac{1}{n_2}\right)}} \tag{31}$$

Using Equation (28)-(31), Z-value is calculated to be 2.635231. The corresponding p-value to this Z-value is 0.004204, which is lower than 0.05, so there is enough to reject the null hypothesis that downward facing mirrors are as likely to experience above median drift as upward facing mirrors (with 95% significance level).

After iterations of different values of c, it was concluded that downward facing mirrors are 13% more likely to experience above median drift (with 95% significance level).